2011-10

Local structure study of vanadium pentoxide 1D-nanostructures

Journal of Nanoparticle Research, Dordrecht : Springer, v. 13, n. 10, p. 4937-4946, Oct. 2011
http://www.producao.usp.br/handle/BDPI/49802

J Nanopart Res (2011) 13:4937–4946
DOI 10.1007/s11051-011-0472-2

RESEARCH PAPER

Local structure study of vanadium pentoxide 1D-nanostructures

W. Avansi · L. J. Q. Maia · C. Ribeiro · E. R. Leite · V. R. Mastelaro

Received: 28 April 2011 / Accepted: 19 June 2011 / Published online: 7 July 2011

Abstract Vanadium pentoxide ($V_2O_5 \cdot nH_2O$) 1D-nanostructures as nanowires and nanorods have been obtained by decomposition of vanadium peroxide in hydrothermal conditions. Electron microscopy, Raman spectroscopy, and X-ray absorption spectroscopy (XAS) were employed to characterize the morphology and the local structure of as-obtained samples. Scanning transmission electron microscopy (STEM) revealed that the diameter of the nanowires and nanorods were found to be 10–20 and 30–40 nm, respectively. The results demonstrated that a combination of Raman and XAS techniques allowed the accurate characterization of the local structure of V_2O_5 1D-nanostructures which are related to different morphologies. Analyses of X-ray absorption near-edge structure (XANES) and extended X-ray absorption fine structure (EXAFS) spectra reveals that the local structure of V in the as-obtained samples is similar to the bulk V_2O_5 (in orthorhombic phase), except for a higher degree of local symmetry within the structure of the VO_5 square pyramid. Additionally, the nanostructures prepared by this technique present a single crystalline nature and could emit visible light at room temperature which is related to the local order of V atoms of the studied samples.

Keywords Vanadium pentoxide · Nanostructures · XAS spectroscopy · Raman spectroscopy · Luminescence

W. Avansi (✉) · C. Ribeiro
Embrapa Instrumentação, Rua Quinze de Novembro 1452, São Carlos 13560-970, SP, Brazil
e-mail: w_avansi@if.sc.usp.br

L. J. Q. Maia
Grupo Física de Materiais—Instituto de Física—UFG, Goiânia, GO, Brazil

E. R. Leite
LIEC—DQ/UFSCAR, Universidade Federal de São Carlos, São Carlos, SP, Brazil

V. R. Mastelaro
Instituto de Física de São Carlos, Universidade de São Paulo, São Carlos, SP, Brazil

Introduction

In the last decades, one-dimensional (1D) nanostructured materials, such as nanowires, nanoribbons, and nanotubes have attracted the interest of many researchers due to their improved properties when compared to similar isotropic structures (Wang and Li 2006; Cademartiri and Ozin 2009; Barth et al. 2010). Among these materials, 1D vanadium pentoxide is an example of a compound which possesses great potential for different applications, such as in photocatalysis (Li et al. 2006), sensors (Leroy et al. 2007; Liu et al. 2005, 2006; Serier et al. 2006), electrochemical (Wang et al. 2005) and optical devices (Yan et al. 2009).

Several strategies were developed to obtain simple and effective methodologies for their synthesis

(Burda et al. 2005; Petkov et al. 2002; Livage 1991, 1998; Yan et al. 2009; Velazquez and Banerjee 2009; Pinna et al. 2003; Liu et al. 2005; Zhou et al. 2008; Niederberger et al. 2000; Li et al. 2006; Avansi et al. 2009; Gao et al. 2008; Glushenkov et al. 2008; Wang and Cao 2006). From that, hydrothermal methods are noteworthy since its possibility to tailor different morphologies by changing few experimental parameters (Avansi et al. 2009; Zhou et al. 2008; Liu et al. 2005; Li et al. 2006). Recently, our research group reported a systematic study using this method for the synthesis of $V_2O_5nH_2O$ nanostructures through the V_2O_5–H_2O_2 route, whose morphology, crystal structure, and water content between the layered structures were regulated by strictly controlling the hydrothermal synthesis variables, avoiding foreign ions or templates and maintaining accurate control of V concentration (Wang and Cao 2006; Avansi et al. 2009).

Because of the potential in several applications of the nanostructured materials, the knowledge about the local structure supports the better understanding of the different properties of these compounds. In fact, several papers correlated some properties of different materials, like photoluminescence, to this aspect (Nakajima et al. 2010; Moreira et al. 2009; Motta et al. 2009).

In this sense, the local structure of 1D $V_2O_5{\cdot}nH_2O$ nanostructures obtained by hydrothermal method was studied by means of X-ray absorption spectroscopy (XAS) and Raman spectroscopy. Photoluminescence (PL) properties of V_2O_5 in different morphologies were evaluated. The correlation between this property and the V_2O_5 micro and nanostructures regarding the local structures is then discussed in order to improve our knowledge about this material.

Experimental section

The synthesis of $V_2O_5{\cdot}nH_2O$ nanostructures obtained in hydrothermal conditions was described in greater detail in Avansi et al. (2009). This synthesis is based on the dissolution of 0.06 M of V_2O_5 micrometric powder (*Alfa Aesar,* 99.995% purity) in distilled water with the addition of 30% H_2O_2 and then subjected to hydrothermal treatment. To obtain different $V_2O_5{\cdot}nH_2O$ nanostructures, the hydrothermal treatment was done in different temperatures. The samples obtained at 180 °C during 24 h of hydrothermal treatment were denoted as SAM01 while the samples obtained at 200 °C for 24 h were denoted as SAM02. The V_2O_5 compound, the precursor material, was characterized as reference compound to compare the structural properties with the as-synthesized materials.

The crystalline structure of the samples was checked by micro-Raman microscopy (WITec, Alpha 300S-CRM200). The spectral excitation was provided by an Ar^+ ion laser, at 514.5 nm laser line and 0.6 mW laser power. The low power laser was chosen to prevent interferences in samples deposited directly on sheet glass, as degradation, dehydration, etc. (Souza et al. 2004).

Local atomic structure around vanadium (V) atoms was studied by X-ray absorption spectroscopy (XAS). The XAS spectra were measured at the V K-edge using the D08B-XAFS2 beam line at the Brazilian Synchrotron Light Laboratory (LNLS). For XAS measurements, the samples were deposited on polymeric membranes and the signal was collected with the sample placed at 90° regarding the X-ray beam. The V K-edge XAS spectra were collected in transmission mode at room temperature using a Si (111) channel-cut monochromator. To provide better energy reproducibility during the spectra collection, the energy calibration of the monochromator was checked during the data collection using a V metal foil. X-ray absorption near-edge spectroscopy (XANES) spectra were measured from 40 eV below and 80 eV above the edge, with an energy step of 0.3 eV near the edge region. Three extended X-ray absorption fine spectroscopy (EXAFS) spectra were measured from 100 eV below and 1.300 eV above the edge, with an energy step of 2 eV integrating during 3 s. The analysis and theoretical calculations of XAS spectra were performed using IFEFFIT package (Ravel and Newville 2005a, b).

Sizes and morphologies were determined by electron microscope using a Zeiss VP Supra 35 equipped with a field emission gun (FE) operating in scanning (SEM) and scanning transmission modes (STEM). The JEOL JEM 2010 URP (operating at 200 keV) was employed in order to obtain a high-resolution transmission electron microscope (HRTEM). FE-STEM and HRTEM images were obtained from samples deposited in thin film form on a copper grid covered with a thin layer of carbon.

Photoluminescence spectroscopy was studied by emission spectra obtained in a Fluorolog FL-322 Horiba/Jobin-Yvon spectrofluorimeter, with a 450 W xenon lamp for steady-state luminescence spectra and a Hamamatsu photomultiplier. The emission was corrected for the spectral response of the monochromators and by the detector using a typical correction spectrum provided by the manufacturer.

Results and discussions

Initially, X-ray diffraction (XRD) patterns were collected for each sample to confirm the successful synthesis. All the patterns (not shown here) confirm the same crystalline phase for all the studied samples, i.e., orthorhombic phase, as expected Avansi et al. (2009). Also as expected, samples SAM01 and SAM02 show, respectively, nanowire-like (Fig. 1a) and nanorod-like (Fig. 1b) morphologies. Figure 1a shows that SAM01 is composed of 10–20 nm width nanowires with micrometric lengths, whereas SAM02 is composed of 30–40 nm width nanorods, Fig. 1b. These morphologies are quite similar to those reported by several authors using different synthesis methods followed by hydrothermal treatment (Gao et al. 2008; Zhou et al. 2005; Liu et al. 2005). Concerning the compound chosen as precursor, V_2O_5 orthorhombic phase, FE-SEM image shows a micro-structured morphology, Fig. 1c, as expected.

The HRTEM images of SAM02, in Fig. 2a and b, show a nanorod with an ordered structure of V_2O_5 orthorhombic phase. As observed in Fig. 2b, the interplanar distance is about 0.60 nm. This distance is consistent with (200) plane in the V_2O_5 orthorhombic phase, as observed in our previous papers (Avansi et al. 2009, 2010). The preferential growth direction of these nanostructures is in [010] plane direction (Avansi et al. 2009, 2010). The HRTEM images in Fig. 2b and their respective Fast Fourier Transform (FFT), Fig. 2c, confirm the single-crystal nature of SAM02. The SAM01 also presents a preferential growth along [010] and single-crystal nature and, therefore, will not be presented here.

To study the crystallographic phase, Fig. 3a and b presents the micro-Raman spectra of the precursor (V_2O_5) and the as-obtained samples SAM01 and SAM02. The precursor Raman spectrum shows bands at 144, 196, 283, 303, 404, 480, 525, 699, and

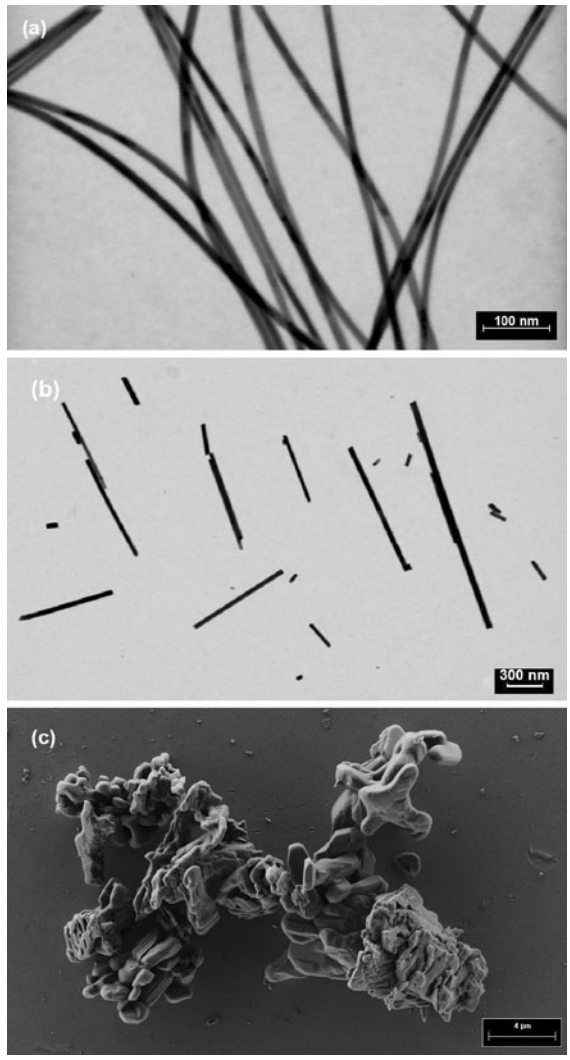

Fig. 1 FE-STEM images of the samples: **a** SAM01, **b** SAM02, **c** FE-SEM images of V_2O_5 employed as precursor

993 cm^{-1}, which are assigned to the crystalline V_2O_5 orthorhombic phase (Abello et al. 1985). The inset of Fig. 3a illustrates the coordination of vanadium with five oxygen in V_2O_5 orthorhombic phase (Stizza et al. 1989). The relative intense low-wavelength peak located around 144 cm^{-1} is attributed to the skeleton bent vibration (B_{3g} mode), while the peaks at 196 and 283 cm^{-1} derive from the bending vibrations of O_3–V–O_4 bond (A_g and B_{2g} modes). The band at 303 cm^{-1} is assigned to A_g species. The peaks located around 404, 525, and 699 cm^{-1} were, respectively, indexed to the bending vibration of V–O_4–V bond (A_g mode), the stretching vibration of V–O_4 bond (A_g mode) and the stretching vibration

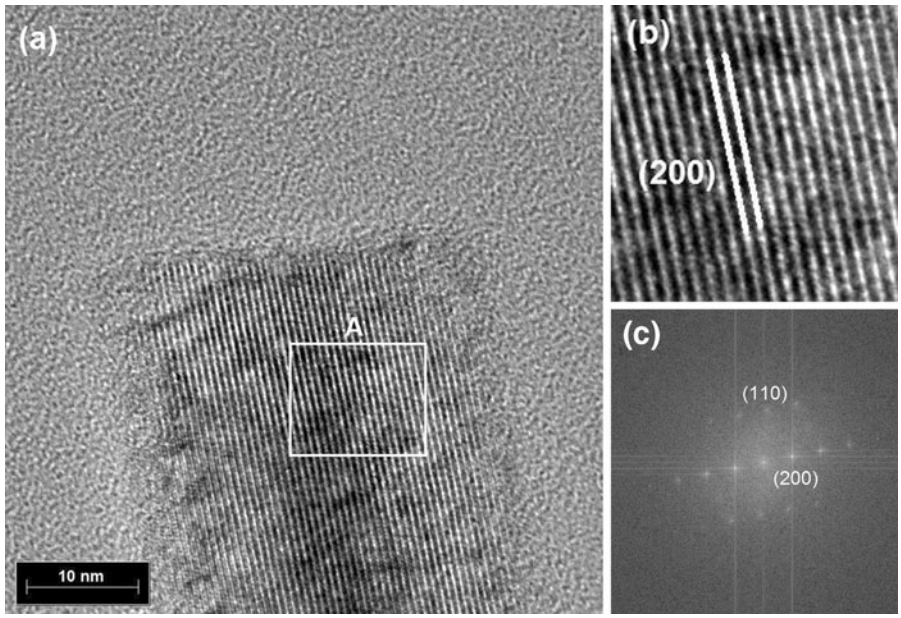

Fig. 2 **a** HRTEM image of the sample obtained at 200 °C for 24 h (SAM02), **b** expanded view of region A, **c** Fast Fourier Transform (FFT) of region A

of V–O_2 bond (B_{2g} and B_{3g} mode) (Zhou and He 2008; Abello et al. 1985; Yan et al. 2009; Ramana et al. 2005). The skeleton bent mode, corresponding to the peak at 144 cm^{-1}, provides an evidence for the layered structure of V_2O_5 orthorhombic phase (Ramana et al. 2005; Abello et al. 1985; Yan et al. 2009; Zhou and He 2008). Furthermore, the narrow peak centered at 993 cm^{-1}, corresponding to the stretching of vanadium connected to oxygen atoms through double bonds (V=O), is also an additional clue to the layer-type structure of V_2O_5 (Zhou and He 2008; Abello et al. 1985; Yan et al. 2009; Ramana et al. 2005). The Raman spectra of SAM01 and SAM02, Fig. 3a, are very similar to the precursor, showing that the long-range order structure is similar to the V_2O_5 orthorhombic phase. Although, in this synthesis condition, the SAM01 and SAM02 contained at room temperature, respectively, 1.0 and 0.5 mol of water, where the higher water content is related to adsorbed water (Avansi et al. 2009). Nevertheless, the expanded view in Fig. 3b clearly shows a shift on the V–O_2 (699 cm^{-1}) and V=O_1 bonds (993 cm^{-1}) vibrations bonds. In both cases, these bands were, respectively, shifted to around 693 and 989 cm^{-1}. These shifts to lower values indicate an increase in V–O_2 and V=O_1 bond-length. According to Mansour et al. (2003b), the V–O bond-lenght is strongly related to the hybridization degree and consequently to the VO_5 square pyramid local structure.

To verify the effect of morphology change on the local order structure of the samples, the X-ray absorption spectroscopy (XAS) technique was employed. Figure 4a and b shows the normalized XANES spectra of the as-obtained SAM01 and SAM02 samples and the micropowder V_2O_5 with orthorhombic phase, used as a reference compound. It is important notice that the XANES spectra were taken with the samples oriented at a 90° angle to the X-ray beam and X-ray polarization effects were not considered. XANES spectra of the as-obtained samples are quite similar to the V_2O_5 reference compound, Fig. 4a, with some differences being observed in the pre-edge region, peak *A* (Fig. 4b). The pre-edge peak is a product of the transition from V 1*s* states to V 3*d* states (Mansour et al. 2003a, b; Stizza et al. 1989). This transition, however, is forbidden by the dipole selection rules in centrosymmetric systems, although it is allowed in noncentrosymmetric systems via hybridization between the V 3*d* and O 2*p* states (Mansour et al. 2002, 2003a, b; Stizza et al. 1989). The intensity of this pre-edge peak showed a strong dependence on the local structure around vanadium atoms, indicated by the degree of distortion of the first oxygen atoms, which influenced

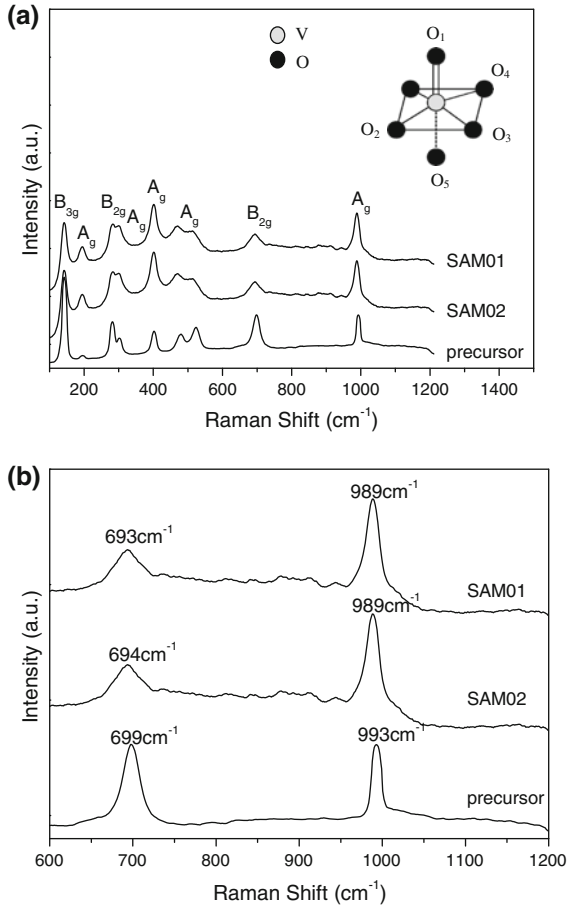

Fig. 3 **a** and **b** Micro-Raman spectra of the precursor and as-prepared samples, SAM01 (180 °C for 24 h) and SAM02 (200 °C for 24 h). *Inset* in **a**: coordination of vanadium with oxygen in V_2O_5 orthorhombic phase (Stizza et al. 1989)

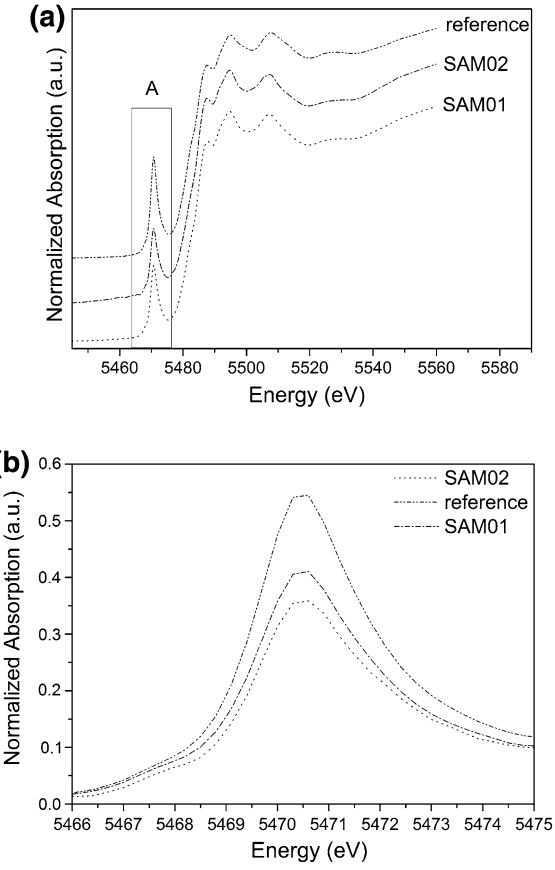

Fig. 4 **a** Normalized Vanadium K-edge XANES spectra and **b** the expanded view of the pre-edge region of normalized XANES of reference compounds (V_2O_5 orthorhombic phase) and the as-obtained SAM01 and SAM02 samples

the degree of hybridization between the O 2*p* and V 3*d* orbitals (Mansour et al. 2003a; Stizza et al. 1989). According to previous works (Mansour et al. 2002; Avansi et al. 2009), the degree of hybridization increase as the V=O distance decreased. As can be observed from Fig. 4b and Table 1, the intensity of the pre-edge peak *A* decreases as the temperature of synthesis increases and it is lower than that of the V_2O_5 reference compound. A decrease in the pre-edge peak intensity suggests an increase in the vanadyl (V=0) distance, which decreases the degree of distortion of the local structure, increasing the local symmetry of the structure within the VO_5 square pyramid (Mansour et al. 2003a). This observation is in good agreement with Raman results. On the other hand, the lower intensity of the pre-edge peak on the XANES spectra of SAM01 when compared to SAM02 and reference compound shows that the local structure of vanadium atoms in the nanostructured samples has a higher degree of symmetry within the VO_5 square pyramid when obtained at higher temperatures.

The edge energy, E_{edge}, like the pre-edge peak energy in the SAM01 and SAM02 samples are similar to that of the V_2O_5 orthorhombic phase, Table 1. The energy of the inflection point at the onset of the pre-edge peak or the main edge is also sensitive to variations in the oxidation state of vanadium (Mansour et al. 2002; Avansi et al. 2009). As can be observed from the results presented in Table 1, the energy position of the pre-edge peak and the vanadium edge of studied samples are quite similar to orthorhombic V_2O_5 phase. This indicates that the oxidation state of vanadium atoms in the

Table 1 Energy position and intensity of pre-edge and edge features of studied samples and orthorhombic V_2O_5 reference compound

Sample	E^{a}_{edge} (eV)	I^{b}_{A} (intensity)	E^{c}_{A} (eV)
SAM01	5481.7	0.40	5470.5
SAM02	5481.9	0.36	5470.5
V_2O_5 (reference)	5481.4	0.54	5470.5

[a] Energy measured at half-height of the normalized XANES spectra

[b] Intensity of pre-edge peak

[c] Energy of pre-edge peak

samples under study was similar to the vanadium atoms in the reference compound, i.e., V^{5+}. From this result, the reduced intensity of the pre-edge peak for the as-obtained samples cannot be attributed to the presence of V in other oxidation state.

To confirm the agreement between XANES and Raman results, quantitative results about the local structure around vanadium atoms were obtained from the analysis on the EXAFS region of the XAS spectra. The experimental V K-edge EXAFS signals $\chi(k)K^1$ and their respective Fourier Transforms (FT) for samples SAM01 and SAM02 and reference compound are shown in Fig. 5a and b.

Variations in V local structure are clearly depicted in the FT shown in Fig. 5b, which displays the radial structure functions for the central absorbing vanadium atom. It is noteworthy since the structure below 1 Å may arise from atomic XAFS and/or multielectron excitations, and it does not usually correspond to real coordination spheres (Mansour et al. 2003b; Giorgetti et al. 2000; Stizza et al. 1989).

The experimental data present three main well-defined peaks, at 1.47, 2.70, and 3.25 Å because of mainly single scattered contribution from coordination spheres of V–O (1st coordination sphere), V–V (2nd sphere) and V–V (3rd sphere), respectively (Mansour et al. 2003b; Giorgetti et al. 2000; Stizza et al. 1989). Since the structure of the third peak contains contributions from a large number of overlapping single as well as multiple-scattered contributions from other paths, the analysis is focused on the first and second coordination spheres. The reference structural parameters used for fitting the reference compound (V_2O_5 orthorhombic phase) has a square pyramidal coordination with an apical vanadyl bond (VO_5) at a distance of 1.586 Å and 4

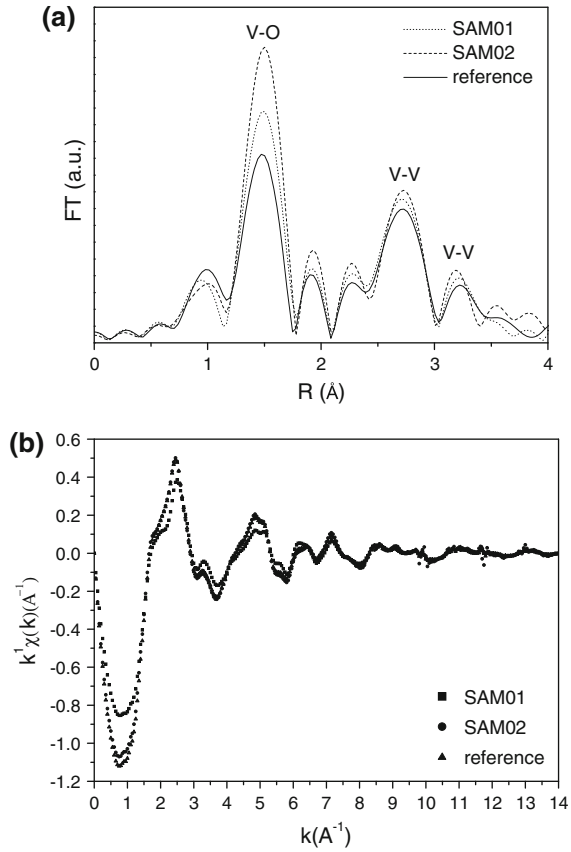

Fig. 5 **a** Experimental uncorrected FT curve of reference compound (V_2O_5), SAM01 and SAM02 EXAFS spectrum. The curves are obtained in the 3.5–14 $Å^{-1}$ k-space using a Hanning window; **b** experimental V K-edge EXAFS signals $\chi(k)K^1$ for the reference compound (V_2O_5), SAM01 and SAM02 samples

V–O bonds at 1.781, 1.878, and 2.022 Å, which form square pyramid basis. The 2nd coordination sphere has V–V bond at 3.019 Å and V–O bond at 2.787 Å (Mansour et al. 2003b; Giorgetti et al. 2000; Stizza et al. 1989).

The best-fitting results for all analyzed samples are reported in Table 2. The good quality could be observed in Fig. 6a and b and by R-factor obtained in this procedure. The fitting procedure outputs three main parameters: distance displacement from theoretical values (ΔR, in Å), Debye–Waller factors (σ^2), and coordination number (CN) related to the V–O and V–V interaction. Two fitting parameters, ΔE_0 and S_0^2, were obtained from the best-fitting for the reference compound and fixed for studied samples. ΔE_0 has been found to be little displaced (0.5 ± 2.1 eV) regarding the edge inflection point,

and S_0^2 values were obtained as 1.1 ± 0.1 and 0.8 ± 0.2 for the first and second shell, respectively.

The amplitude of V–O and V–V correlations on FT for SAM01 and SAM02 are higher than the reference compound, suggesting reduction on the structural disorder degree. Analyzing the Table 2, it is clear that the average V–O distances (ΔR) for the as-obtained samples shifted from reference compound (V_2O_5 orthorhombic phase) to higher values, in good agreement with XANES and Raman results. As reported by Mansour et al. (2002), the local order of V–O coordination sphere directly depends on V–O distance. In this sense, both samples show a decrease in σ^2 when compared to reference compound, and SAM02 has higher symmetry than SAM01. Concerning the first coordination shell around the V atoms, similar coordination numbers (CN) are observed. In fact, for SAM02 a decrease was observed, nevertheless, considering the uncertainty involved, the dimensions of the nanostructures and the fact that the differences in EXAFS spectra were observed for $k < 6\ A^{-1}$ this could not be considered. The second coordination sphere (V–V), which represents the V–V distance within the edge-sharing square pyramids, also presents an increase in average distance with a small increase in σ^2 and similar CN for both samples.

In fact, the higher local symmetry clearly depends on synthesis conditions, which could be related to morphology. However, the hydration state of the samples cannot be related to this difference, since the early reports (Petkov et al. 2002) related the water molecule to O around 2.787 Å, which is not at the distances analyzed here.

Recently, some papers reported the PL properties of V_2O_5 and vanadate compounds (Yan et al. 2009; Wang et al. 2007; Pol et al. 2009; Teramura et al. 2008; Nakajima et al. 2010). Figure 7a shows PL spectra of the as-obtained samples and V_2O_5 micrometric precursor powder, as shown in Fig. 2c. The maximum emissions are observed under the excitation at 510 nm (around 2.43 eV). One sees from Fig. 7a that the nanostructured (SAM01 and SAM02) and microstructured V_2O_5 samples may emit visible light at room temperature showing a PL with broad emission at 540–830 nm (around 2.3–1.5 eV). According to the literature, other interesting effect in PL spectra is the possible presence of sharp peaks

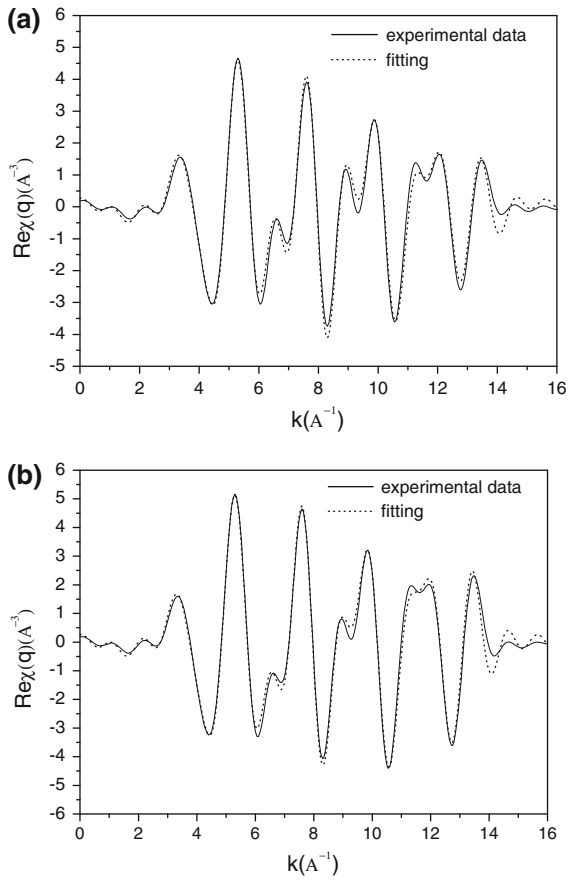

Fig. 6 Comparison between filtered experimental EXAFS data and fits for the as-obtained samples **a** SAM01 and **b** SAM02

Table 2 EXAFS best-fitting results for the as-obtained SAM01 and SAM02 samples, with R-factor equal to 0.002 and 0.003, respectively

Sample	1st shell (V–O)			2nd shell (V–V)		
	CN	ΔR (Å)	σ^2 (Å)	CN	ΔR (Å)	σ^2 (Å)
Reference	5	0.018 ± 0.011	0.004 ± 0.001	4	0.024 ± 0.017	0.005 ± 0.002
SAM01	4.98 ± 1.25	0.029 ± 0.015	0.003 ± 0.001	3.8 ± 1.4	0.029 ± 0.015	0.006 ± 0.002
SAM02	4.30 ± 1.02	0.032 ± 0.016	0.001 ± 0.001	4.1 ± 1.3	0.027 ± 0.007	0.006 ± 0.002

from the V=O vanadyl group vibration involved in the tetrahedral coordination, more prominent under low temperature (Zhang et al. 1998). Since any sharp structure is observed around the peak, we conclude that the oxygen in the V=O bond in studied samples is stable at room temperature. As indicated by Fig. 7b, the PL spectrum can be fitted by two Gaussian peaks centered at 1.88 and 2.08 eV, which correspond to 660 and 596 nm, respectively. The observed visible light emissions cannot be related by the band edge transition where according to some previous papers V_2O_5 nanostructures have a bandgap around 2.3–2.5 eV, i.e., around 500–540 nm (Yan et al. 2009; Beke et al. 2008; Wang et al. 2007).

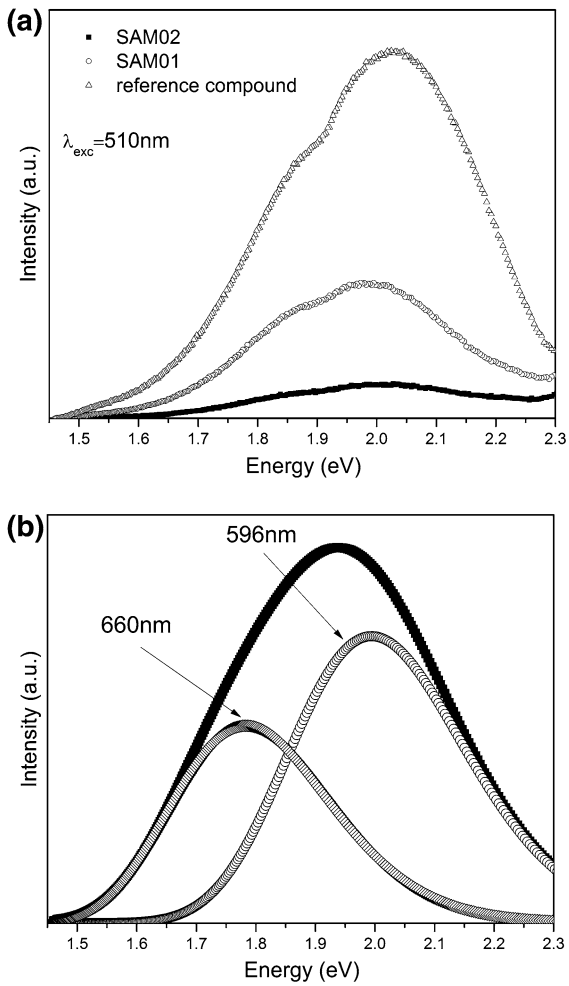

Fig. 7 **a** The room temperature PL spectra of the as-synthesized SAM01 and SAM02 nanostructures and V_2O_5 microstructures; **b** PL spectra of SAM01 deconvoluted

As observed in Fig. 7a, the emission energies remain constant, even with different morphologies and sizes, indicating that the observed visible light emission is not related to these parameters. In fact, the main difference is the PL intensity of the visible light emission, where for V_2O_5 compounds are commonly attributed to defects, such as oxygen vacancies (Diaz-Guerra and Piqueras 2008; Wang et al. 2007; Hu et al. 2009; Yan et al. 2009). Nevertheless, EXAFS results confirm that studied samples exhibit a similar coordination number, i.e., any significant change concerning the first coordination shell around the V atoms can be observed. Since the dependence of local order with photoluminescence properties has been reported for several nanostructures, like for titanates and vanadates (Nakajima et al. 2010; Motta et al. 2009; Moreira et al. 2009; Longo et al. 2008; Zhang et al. 1998), the difference in PL intensity may be related to the local order for V–O sphere, as observed in Raman and XAS results.

Conclusion

This paper demonstrates an accurate characterization of the local structure of 1D $V_2O_5{\cdot}nH_2O$ nanostructures, in orthorhombic phase, by a combination of spectroscopy techniques. The as-obtained V_2O_5 1D nanostructures present a higher local order of V–O coordination sphere than similar microstructures, where this local order depends on morphology of the as-obtained nanomaterials. The results also demonstrate that the $V_2O_5{\cdot}nH_2O$ could emit visible light at room temperature, which the PL properties are directly related to local order of V–O coordination sphere.

Acknowledgments The authors gratefully acknowledge the financial support of the Brazilian research funding agencies FAPESP, CAPES, and CNPq. XAS measurements and HRTEM microscopy facilities were provided by LNLS-Campinas, SP, Brazil.

References

Abello L, Husson E, Repelin Y, Lucazeau G (1985) Structural study of gels of V_2O_5—vibrational spectra of xerogels. J Solid State Chem 56(3):379–389

Avansi W, Ribeiro C, Leite ER, Mastelaro VR (2009) Vanadium pentoxide nanostructures: an effective control of

morphology and crystal structure in hydrothermal conditions. Cryst Growth Des 9(8):3626–3631. doi:10.1021/cg900373f

Avansi W, Ribeiro C, Leite ER, Matelaro VR (2010) Growth kinetics of vanadium pentoxide nanostructures under hydrothermal conditions. J Cryst Growth 312:3555–3559

Barth S, Hernandez-Ramirez F, Holmes JD, Romano-Rodriguez A (2010) Synthesis and applications of one-dimensional semiconductors. Prog Mater Sci 55 (6):563–627. doi:10.1016/j.pmatsci.2010.02.001

Beke S, Giorgio S, Korosi L, Nanai L, Marine W (2008) Structural and optical properties of pulsed laser deposited V2O5 thin films. Thin Solid Films 516(15):4659–4664. doi:10.1016/j.tsf.2007.08.113

Burda C, Chen X, Narayanan R, El-Sayed MA (2005) Chemistry and properties of nanocrystals of different shapes. Chem Rev 105(4):1025–1102

Cademartiri L, Ozin GA (2009) Ultrathin nanowires—a materials chemistry perspective. Adv Mater 21(10):1013–1020

Diaz-Guerra C, Piqueras J (2008) Thermal deposition growth and luminescence properties of single-crystalline V_2O_5 elongated nanostructures. Cryst Growth Des 8(3):1031–1034. doi:10.1021/cg070612w

Gao SK, Chen YZ, Luo HY, Jiang LL, Ye BH, Wei MD, Wei KM (2008) Single-crystal vanadium pentoxide nanowires. J Nanosci Nanotechnol 8(7):3500–3503. doi:10.1166/jnn.2008.137

Giorgetti M, Passerini S, Smyrl WH, Berrettoni M (2000) Evidence of bilayer structure in V_2O_5 xerogel. Inorg Chem 39(7):1514–1517

Glushenkov AM, Stukachev VI, Hassan MF, Kuvshinov GG, Liu HK, Chen Y (2008) A novel approach for real mass transformation from V_2O_5 particles to nanorods. Cryst Growth Des 8(10):3661–3665. doi:10.1021/cg800257d

Hu Y, Li ZC, Zhang ZJ, Meng DQ (2009) Effect of magnetic field on the visible light emission of V_2O_5 nanorods. Appl Phys Lett 94(10). doi:10.1063/1.3095502

Leroy CM, Achard MF, Babot O, Steunou N, Masse P, Livage J, Binet L, Brun N, Backov R (2007) Designing nanotextured vanadium oxide-based macroscopic fibers: application as alcoholic sensors. Chem Mater 19:3988–3999. doi:10.1021/cm0711966

Li BX, Xu Y, Rong GX, Jing M, Xie Y (2006) Vanadium pentoxide nanobelts and nanorolls: from controllable synthesis to investigation of their electrochemical properties and photocatalytic activities. Nanotechnology 17(10):2560–2566. doi:10.1088/0957-4484/17/10/020

Liu JF, Wang X, Peng Q, Li YD (2005) Vanadium pentoxide nanobelts: highly selective and stable ethanol sensor materials. Adv Mater 17(6):764. doi:10.1002/adma.200400993

Liu JF, Wang X, Peng Q, Li YD (2006) Preparation and gas sensing properties of vanadium oxide nanobelts coated with semiconductor oxides. Sensors Actuators B 115(1):481–487. doi:10.1016/j.snb.2005.10.012

Livage J (1991) Vanadium pentoxide gels. Chem Mater 3(4):578–593

Livage J (1998) Synthesis of polyoxovanadates via "chimie douce". Coord Chem Rev 178:999–1018

Longo VM, de Figueiredo AT, de Lazaro S, Gurgel MF, Costa MGS, Paiva-Santos CO, Varela JA, Longo E, Mastelaro VR, De Vicente FS, Hernandes AC, Franco RWA (2008) Structural conditions that leads to photoluminescence emission in SrTiO3: an experimental and theoretical approach. J Appl Phys 104(2). doi:10.1063/1.2956741

Mansour AN, Dallek S, Smith PH, Baker WM (2002) Thermogravimetry and X-ray absorption spectroscopy study of heated $V_2O_5{\cdot}nH_{(2)}O$ aerogels and ambigels. J Electrochem Soc 149(12):A1589–A1597. doi:10.1149/1.1517284

Mansour AN, Smith PH, Baker WM, Balasubramanian M, McBreen J (2003a) A comparative in situ X-ray absorption spectroscopy study of nanophase V_2O_5 aerogel and ambigel cathodes. J Electrochem Soc 150(4):A403–A413. doi:10.1149/1.1554911

Mansour AN, Smith PH, Baker WM, Balasubramanian M, McBreen J (2003b) Comparative in situ X-ray absorption spectroscopy study of nanophase V_2O_5 aerogel and ambigel cathodes (vol 150, pg A403, 2003). J Electrochem Soc 150(6):L13–L13. doi:10.1149/1.1574327

Moreira ML, Paris EC, do Nascimento GS, Longo VM, Sambrano JR, Mastelaro VR, Bernardi MIB, Andres J, Varela JA, Longo E (2009) Structural and optical properties of CaTiO3 perovskite-based materials obtained by microwave-assisted hydrothermal synthesis: an experimental and theoretical insight. Acta Mater 57(17):5174–5185. doi:10.1016/j.actamat.2009.07.019

Motta FV, de Figueiredo AT, Longo VM, Mastelaro VR, Freitas AZ, Gomes L, Vieira ND, Longo E, Varela JA (2009) Disorder-dependent photoluminescence in $Ba_{0.8}Ca_{0.2}TiO_3$ at room temperature. J Lumin 129(7):686–690. doi:10.1016/j.jlumin.2009.01.014

Nakajima T, Isobe M, Tsuchiya T, Ueda Y, Manabe T (2010) Photoluminescence property of vanadates M2V2O7 (M: Ba, Sr and Ca). Opt Mater 32(12):1618–1621. doi:10.1016/j.optmat.2010.05.021

Niederberger M, Muhr HJ, Krumeich F, Bieri F, Gunther D, Nesper R (2000) Low-cost synthesis of vanadium oxide nanotubes via two novel non-alkoxide routes. Chem Mater 12(7):1995–2000

Petkov V, Trikalitis PN, Bozin ES, Billinge SJL, Vogt T, Kanatzidis MG (2002) Structure of $V_2O_5{\cdot}nH_{(2)}O$ xerogel solved by the atomic pair distribution function technique. J Am Chem Soc 124(34):10157–10162. doi:10.1021/ja026143y

Pinna N, Wild U, Urban J, Schlogl R (2003) Divanadium pentoxide nanorods. Adv Mater 15(4):329–331

Pol VG, Pol SV, Calderon-Moreno JM, Gedanken A (2009) Core-shell vanadium oxide-carbon nanoparticles: synthesis, characterization, and luminescence properties. J Phys Chem C 113(24):10500–10504. doi:10.1021/jp902503w

Ramana CV, Smith RJ, Hussain OM, Massot M, Julien CM (2005) Surface analysis of pulsed laser-deposited V_2O_5 thin films and their lithium intercalated products studied by Raman spectroscopy. Surf Interface Anal 37(4):406–411. doi:10.1002/sia.2018

Ravel B, Newville M (2005a) ATHENA and ARTEMIS: interactive graphical data analysis using IFEFFIT. Physica Scripta T115:1007–1010

Ravel B, Newville M (2005b) ATHENA, ARTEMIS, HEPHAESTUS: data analysis for X-ray absorption spectroscopy using IFEFFIT. J Synchrotron Radiat 12:537–541. doi:10.1107/s0909049505012719

Serier H, Achard MF, Babot O, Steunou N, Maquet J, Livage J, Leroy CM, Backov R (2006) Designing the width and texture of vanadium oxide macroscopic fibers: towards tuning mechanical properties and alcohol-sensing performance. Adv Funct Mater 16(13):1745–1753. doi:10.1002/adfm.200600044

Souza AG, Ferreira OP, Santos EJG, Mendes J, Alves OL (2004) Raman spectra in vanadate nanotubes revisited. Nano Lett 4(11):2099–2104. doi:10.1021/nl0488477

Stizza S, Mancini G, Benfatto M, Natoli CR, Garcia J, Bianconi A (1989) Structure of oriented V_2O_5 gel studied by polarized X-ray-absorption spectroscopy at the vanadium K edge. Phys Rev B 40(18):12229–12236

Teramura K, Hosokawa T, Ohuchi T, Shishido T, Tanaka T (2008) Photoactivation mechanism of orthovanadate-like (V=O)O-3 species. Chem Phys Lett 460(4–6):478–481. doi:10.1016/j.cplett.2008.06.025

Velazquez JR, Banerjee S (2009) Catalytic growth of single-crystalline V_2O_5 nanowire arrays. Small 5(9):1025–1029. doi:10.1002/smll.200801278

Wang Y, Cao G (2006) Synthesis and enhanced intercalation properties of nanostructured vanadium oxides. Chem Mater 18(12):2787–2804

Wang X, Li Y (2006) Solution-based synthetic strategies for 1-D nanostructures. Inorg Chem 45(19):7522–7534

Wang Y, Takahashi K, Shang HM, Cao GZ (2005) Synthesis and electrochemical properties of vanadium pentoxide nanotube arrays. J Phys Chem B 109(8):3085–3088. doi:10.1021/jp044286w

Wang YQ, Li ZC, Sheng X, Zhang ZJ (2007) Synthesis and optical properties of V_2O_5 nanorods. J Chem Phys 126(16). doi:10.1063/1.2722746

Yan B, Liao L, You YM, Xu XJ, Zheng Z, Shen ZX, Ma J, Tong LM, Yu T (2009) Single-crystalline V_2O_5 ultralong nanoribbon waveguides. Adv Mater 21(23):2436. doi:10.1002/adma.200803684

Zhang SG, Higashimoto S, Yamashita H, Anpo M (1998) Characterization of vanadium oxide/ZSM-5 zeolite catalysts prepared by the solid-state reaction and their photocatalytic reactivity: in situ photoluminescence, XAFS, ESR, FT-IR, and UV-vis investigations. J Phys Chem B 102(29):5590–5594

Zhou B, He DY (2008) Raman spectrum of vanadium pentoxide from density-functional perturbation theory. J Raman Spectrosc 39(10):1475–1481. doi:10.1002/jrs.2025

Zhou GT, Wang XC, Yu JC (2005) Selected-control synthesis of NaV_6O_{15} and $Na_2V_6O_{16}{\cdot}3H_{(2)}O$ single-crystalline nanowires. Cryst Growth Des 5(3):969–974. doi:10.1021/cg0496686

Zhou F, Zhao XM, Yuan CG, Li L (2008) Vanadium pentoxide nanowires: hydrothermal synthesis, formation mechanism, and phase control parameters. Cryst Growth Des 8(2):723–727. doi:10.1021/cg060816x